

**This article has been published in: Injury. 2018 Sep;49 Suppl 2:S3-S10.**

**Title:** Assessing bone quality through mechanical properties in postmenopausal trabecular bone

**Authors:** Manuel Toledano<sup>1</sup>, Manuel Toledano-Osorio<sup>1</sup>, Enrique Guerado<sup>2</sup>, Enrique Caso<sup>3</sup>, Estrella Osorio<sup>1\*</sup>, Raquel Osorio<sup>1</sup>.

**Institution:** <sup>1</sup>University of Granada, Faculty of Dentistry, Dental Materials Section.

<sup>2</sup>Department of Orthopaedic Surgery and Traumatology. Hospital Universitario Costa del Sol. University of Malaga. Marbella. Malaga. Spain.

<sup>3</sup>Research Unit. Hospital Universitario Costa del Sol. University of Malaga. Marbella. Malaga. Spain.

**Address:** <sup>1</sup>University of Granada, Faculty of Dentistry, Dental Materials Section. Colegio Máximo de Cartuja s/n 18071 Granada. Spain.

<sup>2,3</sup> Hospital Universitario Costa del Sol. University of Malaga. Dual carriageway Km 187, 29603 Marbella. Malaga. Spain

\*Corresponding author: Prof. Estrella Osorio

University of Granada, Faculty of Dentistry  
Dental Materials Section  
Colegio Máximo de Cartuja s/n  
18071 – Granada - Spain.  
Tel.: +34 958243793  
Email: meosorio@ugr.es

## **Abstract**

**Background:** The inner structure of trabecular bone is a result of structural optimisation provided by remodeling processes. Changes in hormonal status related to menopause cause bone tissue loss and micro-architectural deterioration with a consequent susceptibility to fracture. Accumulation of micro-damage in bone, as a function of the rate of production and rate of repair, underlies the development of stress fractures, increasing fragility associated to age and osteoporosis, especially in transmenopausal women. **Patients and Methods:** Quasi-static and nano-dynamic mechanical characterisation were undertaken in trabecular bone from femoral neck biopsies of postmenopausal women. AFM complementary studies were performed to determine nano-roughness (SRa) and the fibrils width of collagen. Nanoindentations were used to quantify transmenopausal changes in intrinsic mechanical properties of trabecular bone: hardness ( $H_i$ ), modulus of Young ( $E_i$ ), complex modulus ( $E^*$ ), tan delta ( $\delta$ ), storage modulus ( $E'$ ) and loss modulus ( $E''$ ). **Results:** As result of the quasi-static measurements, 0.149 (0.036) GPa and 2.95 (0.73) GPa of  $H_i$  and  $E_i$  were obtained, respectively. As result of the nano-dynamic measurements, 17.94 (3.15), 0.62 (0.10), 13.79 (3.21) and 6.39 (1.28) GPa of  $E^*$ ,  $\tan(\delta)$ ,  $E'$  and  $E''$  were achieved, respectively. 101.07 SRa and 831.28 nm of fibrils width were additionally obtained. **Conclusion:** This study poses a first approach to the measurement of bone quality in postmenopausal trabecular bone by combining quasi-static, nano-DMA analysis and tribology of dentin surface through AFM characterization

**Key words:** Trabecular bone, static, dynamic, mechanic, menopause.

## Introduction

Bone is a natural composite material consisting primarily of three phases: mineral, organic and water. They are organised into a complex hierarchical structure, and are not independent of each other, but rather work in harmony to determine the biomechanical properties of bone<sup>1</sup>. The macro-scale mechanical properties of the bone are controlled by both the structural organisation of the micro and nano-scale constituents as well as the intrinsic mechanical properties of these constituents across the different length scales<sup>2</sup>. There are generally two types of bone tissue: trabecular and cortical. Trabecular bone is a highly porous structure that fills the proximal and distal ends of all bones (*e.g.*, femur) and is also present as a filler in other bones (*e.g.* vertebral bodies and both maxilar bones), providing structural support and flexibility<sup>3</sup>. The mechanical properties of the trabecular bone depend on volume fraction, microarchitecture, and trabecular tissue material properties. Characterisation of the latter and its role in trabecular bone mechanical behavior has potential clinical and biological importance<sup>4</sup>.

Although understanding static mechanical properties is truly beneficial, considering that the majority of bone fractures occur under dynamic conditions such as accidents or sporting activities for the young and falls for the elderly, it is also very important to understand the dynamic mechanical behavior of bone<sup>1</sup>. Atomic force microscopy (AFM) nano-indentation is the most commonly applied means of testing the mechanical properties of materials or substrates<sup>5</sup>, and it was deemed to be a suitable method for the determination of the visco-elasticity of hard tissues<sup>6,7</sup>, at nanoscale<sup>8</sup>. Clinically, knowledge of the elastic and failure properties of trabecular tissue obtained by nanoindentation could be used to investigate the effects of drugs treatment, aging, and disease at the tissue level. Measurements have high spatial resolution due to small indenter tip radius, are nondestructive on a macroscopic level, and are sensitive to

material anisotropy<sup>9,10,11,12</sup>. Viscoelastic materials dissipate energy when loaded. In bone, this is important for its fracture resistance under dynamic or impact loading<sup>13</sup>. From composite materials perspectives, the biomechanical properties of bone are dependent on the quality and the spatial arrangement of its constituents<sup>14</sup>. As polymers, bone components exhibit time-dependent behavior representative of non-linearly viscoelastic media. Viscoelasticity is the type of behavior attributed to materials that exhibit both elastic and viscous qualities under deformation. Viscoelastic materials, as bone deform according to a combination of these properties and, as such, exhibit time-dependent strain<sup>15</sup>.

Trabecular tissue properties are of great interest in the etiology of osteoporosis since it is widely speculated that this aspect of bone “quality” does affect fracture risk<sup>4</sup>. Lower heterogeneity of trabecular bone of the osteoporotic patients may contribute to fracture susceptibility due to a lowered ability to prevent crack propagation<sup>16</sup>. The importance of assessment of mechanical properties at the tissue level, *i.e.*, at the level of single trabeculae can be demonstrated using indirect determination of trabecular bone mechanical properties from high-resolution images of its viscoelastic performance. These models can be used to study the relation between the microstructure and overall properties at the tissue levels. Moreover, nanoindentation, as a measurement tool for very local mechanical properties is able to distinguish this variation in different content (interstitial bone has a larger mineral content compared to the bone on the trabecular surface). Thus, modulus mapping shows the trend of larger stiffness in core, meanwhile smaller values are measured in superficial areas<sup>3</sup>. Scanning probe microscopes and, in particular, the AFM have facilitated the imaging and analysis of biological surfaces with little or no sample preparations<sup>17</sup>. AFM operates in a near field with a sharp probe by scanning, enabling characterisation of three-dimensional surface morphology with minimal sample

preparation and high resolution. AFM has been widely used to visualise the bone matrix and to determine the spatial relationship between mineral and collagen and their morphology/topology as well <sup>8</sup>. By integrating AFM and nano-dynamic mechanical analyser (nano-DMA), both morpho and nanomechanical properties can be obtained. In particular, biological sample systems resemble complex biochemical and biophysical architectures<sup>16</sup>.

At present, studies addressing the association between quasi-static and dynamic nano-indentation with surface roughness and fibril diameter in human trabecular bone are lacking. The goal of the present study was to propose a study protocol on trabecular bone, based on nanoindentation and AFM characterisation, in order to assess degenerative bone diseases and bone quality with the aim of evaluating new therapies.

## **Material and Methods**

### *Femoral neck biopsy specimens*

Study subjects were hip fracture patients undergoing surgery for total hip replacement, and the specimens were retrieved from the base of the femoral neck. Subjects consented to undergo a femoral neck biopsy. All protocols were approved by the Institutional Review Board, prior to obtaining biopsy samples. These samples were then kept immersed in a phosphate -buffered saline (PBS) solution (pH 7.4) and stored frozen at -20°C <sup>18</sup>. The biopsy specimens were processed in epoxy-resin<sup>19,20</sup>.

### *Nanoindentation*

To prepare the specimens for dynamic nanoindentation (nano-DMA), the epoxy-resin-embedded biopsy specimens that were used to generate sections, were further polished with different diamond pastes, from 10 µm to 0.1 µm in diameter, to obtain

smooth surfaces. Measurements were performed on randomly selected femoral specimens and ~4-5 different trabeculae from each sample <sup>21,22</sup>.

Three sections of epoxy-resin-embedded bone were submitted to nano-DMA to perform the modulus mapping. Property mappings were conducted using a HysitronTi 950 nanoindenter (Hysitron, Inc., Minneapolis, MN) equipped with a commercial nano-DMA package. The nanoindenter was a Berkovich (three-sided pyramidal) diamond indenter tip (tip radius ~20 nm). The nanoindenter tip was calibrated against a fused quartz sample using a quasistatic force setpoint of 5  $\mu\text{N}$  to maintain contact between the tip and the sample surface. Based on a calibration-reduced modulus value of  $1.1400\text{E}+03 \text{ N/mm}^2$  for the fused quartz, the best-fit spherical radius approximation for tip was found to be 150 nm, for the selected nano-DMA scanning parameters. Trabecular struts near the centre of the biopsy were chosen from the optical image for testing. Modulus mapping of our samples was conducted by imposing a quasistatic force setpoint,  $F_q=5 \mu\text{N}$ , to which it was superimposed a sinusoidal force of amplitude  $F_A=1.8 \mu\text{N}$  and frequency  $f=200 \text{ Hz}$ . The resulting displacement (deformation) at the site of indentation was monitored as a function of time. Data from regions approximately  $30 \times 30 \mu\text{m}$  in size were collected using a scanning frequency of 0.2 Hz. Specimens were scanned in a hydrated state.

Under steady conditions (application of a quasistatic force) the indentation modulus of the tested sample,  $E$ , was obtained by application of different models that relate the indentation force,  $F$ , and depth,  $D$ . <sup>23</sup>. Most of these theories assumed proportionality between the force and the indentation modulus:

$$F = g(D)E \Rightarrow E = \frac{F}{g(D)}, \quad (1)$$

where  $g(D)$  is a function on the indentation depth, which depends on the geometry of the probe of the indenter. For example, for a spherical probe, the Hertzian contact theory predicts <sup>24,25</sup>:

$$g(D) = \frac{4R^{1/2}D^{3/2}}{3(1-\nu^2)} \quad (2)$$

In this equation  $R$  is the radius of the spherical probe and  $\nu$  is the Poisson's ratio of the tested sample. As mentioned above, in nano-DMA experiments an oscillatory force is superimposed to a quasistatic force:

$$F = F_q + F_A \sin(2\pi ft) \quad (3)$$

with  $t$  being the time. Under this imposed force, the indentation depth takes the following form:

$$D = D_q + D_A \sin(2\pi ft - \delta) \quad (4)$$

This means that the indentation depth also oscillates around a quasistatic value, with the same frequency that the oscillating force and delayed by a phase lag  $\delta$ . In the limit of  $F_A \ll F_q$  we can expand equation (1) to a first order Taylor approximation, to obtain:

$$F_q + F_A \sin(2\pi ft) = g(D_q)E + g'(D_q)|E^*|D_A \sin(2\pi ft - \delta) \quad (5)$$

In this equation,  $g'$  is the first derivative of  $g$ , and  $E^*$  is the complex dynamic indentation modulus. Now, it can be equaled the time-dependent terms and changed the time origin, to write:

$$F_A \sin(2\pi ft + \delta) = g'(D_q)|E^*|D_A \sin(2\pi ft) \quad (6)$$

Now, the oscillating force can be decomposed into two terms, the in-phase term,  $F'$ , and the out-of-phase term,  $F''$ <sup>26</sup>:

$$\begin{aligned} F_A \sin(2\pi ft + \delta) &= F_A \cos \delta \sin(2\pi ft) + F_A \sin \delta \cos(2\pi ft) = \\ &= F_A' \sin(2\pi ft) + F_A'' \cos(2\pi ft) = F' + F'' \end{aligned} \quad (7)$$

Then, from this decomposition two dynamics moduli can be extracted:

$$E' = |E^*| \cos \delta = \frac{F_A \cos \delta}{g'(D_q)D_A} = \frac{F_A'}{g'(D_q)D_A}, \quad (8)$$

which is the in-phase or storage (elastic) modulus.

$$E'' = |E^*| \sin \delta = \frac{F_A \sin \delta}{g'(D_q)D_A} = \frac{F_A''}{g'(D_q)D_A}, \quad (9)$$

which is the out-of-phase or loss (viscous) modulus.

For the quasi-static nanoindentation with the Berkovich diamond indenter, ten indentations with a peak of load of 4000 nN and a time function of 10 s were performed on the methylmethacrylate-embedded biopsy specimens. From this test, the nanoindentation modulus ( $E_i$ ) of the samples was obtained. This nanoindentation modulus is usually referred to as Young's modulus in the literature, which should not be confounded with the Young's modulus obtained at the macroscopic level by traction/compression experiments. The indenter was progressively (at a constant rate) pressed over the sample up to a peak load of 4000 Mn (loading part of the experiment) and, afterwards, the load was progressively released to zero value (unloading part of the experiment). From these tests the load,  $F$ , was obtained as a function of the penetration depth,  $h$ , of the indenter in the sample. From the slope of these load-vs.-depth curves the nanoindentation modulus (Young's modulus) can be obtained by application of different theoretical models<sup>23,27</sup>. One of these is the Oliver-Pharr method, which is based on a continuum, isotropic, homogeneous elastic contact model to determine the reduced modulus,  $E_r$ . In this model the slope,  $S$ , of the unloading portion of the load-vs. depth data is used to obtain  $E_r$  according to the following equation<sup>27</sup>:

$$S = \frac{dF}{dh} = \frac{2}{\sqrt{\pi}} E_r \sqrt{A}, \quad (10)$$

where  $A$  is the projected contact area of the hardness impression of the indenter. Then,  $E_i$  of the sample is obtained through the following expression:

$$\frac{1}{E_r} = \frac{(1-\nu_{ind}^2)}{E_{ind}} + \frac{(1-\nu_i^2)}{E_i}, \quad (11)$$

In this expression “*i*” subscript refers to the tested sample and “*ind*” subscript to the indenter.  $\nu$  and  $E$  are the Poisson’s ratio and the Young’s modulus, respectively. For hard materials, as dentin, Usually,  $E_{ind} \gg E_i$  and, thus, the contribution of the indenter in equation (2) can be neglected.

Young’s modulus values were automatically calculated (Triboscan Quasi version 8.4.2.0 Hysitron, Inc).

#### *Roughness assessments and Fibril diameter*

An atomic force microscope (AFM Nanoscope V, Digital Instruments, Veeco Metrology group, Santa Barbara, CA, USA) was employed in this study for topography analysis. The imaging process was undertaken inside a wet cell in a fully hydrated state, using the tapping mode, with a calibrated vertical-engaged piezo-scanner (Digital Instrument, Santa Barbara, CA, USA). A 10-nm-radius silicon nitride tip (Veeco) was attached to the end of an oscillating cantilever that came into intermittent contact with the surface at the lowest point of the oscillation. Changes in vertical position of the AFM tip at resonance frequencies near 330 kHz provided the height of the images registered as bright and dark regions. 30 x 30  $\mu\text{m}$  digital images were recorded with a slow scan rate (0.1 Hz). For each image, 5 randomised boxes (3 x 3  $\mu\text{m}$ ) were created for examination of the surface roughness of the trabecular bone. Nanoroughness ( $R_a$ , in nanometers) was measured with proprietary software (Nanoscope Software, version V7).

Five phase images and five three-dimensional (3D) digital images were captured for each specimen. Assembled in a single user interface, NanoScopeAnalysis.Ink software served as a semi-automatic analysis tool capable of measuring several

geometrical properties (length, volume and angles). NanoScope Analysis can open image data files from NanoScope (v5.30v2). The selected image was loaded in the main panel, so individual complexes can be measured. Each complex was labelled with a specific alphanumeric identifier, appearing in the adjacent window for volume and length analysis. Fibrils width were estimated by measuring directly one part of the fibril with the line tool.

Collagen fibril diameter was determined by section analysis using data that had been modified only by plane fitting. Five fibrils were analysed from each image. Measurements were corrected for tip broadening<sup>17</sup> by the equation  $e=2r$ , where  $e$  is the error in the horizontal dimension and  $r$  is the tip's radius<sup>28</sup>.

## Results

The values of viscoelastic properties, *i.e.*, nano-DMA analysis, of the sample corresponding to trabecular bone from a femoral neck biopsy, concerning the complex (17.94 GPa), loss (6.39 GPa), storage moduli (13.75 GPa) and tan delta (0.62 GPa) are shown in Table 1 and Figure 1. Table 1 also shows nanoroughness (SRa) (101.07 nm) and fibrils width (831.28 nm) values at the surface of the trabecular bone specimen, as well as the nanohardness (0.145 GPa) and modulus of Young (2.95 GPa) at the same surface. Atomic force microscopy (AFM) analysis of the trabecular bone are shown in Figure 2. They show different mineral deposits. Characteristic zones of mineral depleted areas and collagen fibers can also be observed.

## Discussion

Hormonal changes related to menopause can cause bone mass loss and a decrease in bone mineral density, and this led to the hypothesis that the bone intrinsic mechanical properties in menopausal women would be “low quality” and prone to fracture.

Microarchitecture is a result of increased remodeling activity and partially contributes to fragility. However, possible accompanying changes in the intrinsic material properties of the bone present after remodeling have not yet been assessed. Hengsberger *et al.*<sup>30</sup> detected a decrease in elastic modulus and hardness of trabecular bone from ovariectomised rats. Wang *et al.*<sup>31</sup> found, on human cancellous bone, significant differences in elastic modulus and hardness which became associated with bone formation rates but fracture was noticed, suggesting that remodeling resulted in decreased mineralisation.

Nanoindentation has been used widely in the biomechanics field to characterise intrinsic material properties of many type tissues. For example, it has been used to study the elastic anisotropy of human cortical bone secondary osteons<sup>32</sup>. It has also been used to study the elastic properties of microstructural components of bone tissue<sup>33,34,35,29,36,37,38</sup>. Ferguson *et al.*<sup>39</sup> combined nanoindentation and quantitative backscattered electron imaging to correlate tissue composition and elasticity on articular calcified cartilage and the immediate subchondral bone in normal and osteoarthritic human femoral heads. Bembey *et al.*<sup>40</sup> examined the effect of bone hydration state on mechanical response as measured by nanoindentation. They found that a hydration increase was associated with a decrease in stiffness, while a hydration decrease resulted in an increase in bone tissue stiffness.

Nanoindentation is attractive because measurements are uniquely capable of characterizing the mechanical response of bone at the submicrostructural level, thus providing mechanical properties of individual bone constituents<sup>2</sup>. In the present study, the quasi-static behavior analysis showed 0.145 GPa of hardness (Eq. 10) and 2.95 GPa of Young's modulus (Eq.11) values (Table 1). Polly *et al.* (2012) achieved wider ranges of both hardness (0.370 to 0.835 GPa) and modulus of Young (14.23 to 14.51 GPa),

respectively. Rho *et al.* (1997) reported on human trabecular bone values of 14.7 and 0.468 GPa for indentation modulus and hardness, respectively. They stated that the value of Young's modulus for individual trabeculae is significantly greater than the widely used value of  $E = 5.4$  GPa obtained by microbending testing. Generally, values reported for bone properties in the literature vary, mainly due to differences between the studies in anatomical location, hydration/embedding techniques, and test parameters. Therefore, results must be interpreted in the context of the methods used to obtain, store, and test the specimens. The intratrabecular variation in intrinsic material properties may have also affected nanoindentation measurements; variations may, in addition, be due to testing nanoscale structures in a hierarchical organised material that extends to the micro level <sup>2</sup>.

Discrepancy among studies is mainly due to the presence of artifacts. The low elastic modulus of trabecular tissue reported in the former studies is most likely due to the measurement of transverse modulus of the anisotropic tissue, spatial sampling and anatomical site-dependence <sup>4</sup>. The understanding of measurement limitations and complexities has grown as the technique has been applied to bone. Researchers have investigated various effects of surface roughness <sup>41</sup> and contact area <sup>42</sup> on measured nanomechanical properties of bone. However, the viscoelastic properties of bone have been only recently explored <sup>43,44</sup>. In the present study after the AFM analysis 101.07 SRA of mean surface roughness values were obtained (Table 1). Polly *et al.* (2012) achieved approximately 50 nm of local roughness, but comparisons are difficult due to the different methodology that was undertaken. The nano-DMA analysis shows that the dampening (or viscous) behavior of the tissue is much more sensitive to the structural changes that occur with function than the quasi-static behavior <sup>45</sup>. Thereby, it requires the capacity to absorb mechanical shock waves and alleviate stresses at these locations in order to prevent crack propagation across the boundary between the two phases of bone. In fact, most

fractures occur under dynamic loading conditions. A better understanding of the viscoelastic behavior of bone would help to further elucidate the mechanisms of such fractures.

The resistance of the trabecular bone to dynamic deformation, given by the value of the complex modulus ( $E^*$ ) (Eqs. 5,6) attained 17.94 GPa (Table 1). Higher complex modulus correlates well with higher stiffness<sup>46</sup>, and was in correspondence with the mixture of yellow and green areas (Fig 1A), mostly concentrated at the top of the image. Tissue mineralisation (Fig. 2) and stiffness were higher near or at the interior of the trabeculae and decreased at locations closer to the trabecular surface<sup>2</sup>. The nano-DMA scanning analysis of trabecular bone permitted observation of zones with high complex modulus close to areas of low modulus (Fig. 1E), which might hinder the dissipation of energy through the interface<sup>47</sup>. Low modulus regions (Fig. 1A, purple/blue areas) lead to stress concentration in relatively high elastic modulus regions<sup>48</sup> (Fig. 1A, red areas), originating microdamage accumulation<sup>49</sup> and may produce focal pockets of damage where microcracks may appear within a single trabecula. The existence of this kind of cracks in bone has been verified by scanning electron and confocal microscopy<sup>49</sup>.

The ratio of the dissipated energy to the stored energy in the system enables its elastic recoil, ( $E''/E'$ ), *i.e.*, the  $\tan \delta$ <sup>50</sup> was 0.62 GPa (Table 1). Tan delta ( $\delta$ ) (Eqs. 4,5), often called damping, loss factor or loss tangent is the ratio of the loss to the storage modulus, and describes the relative amount of energies stored/returned and lost by a specimen during mechanical deformation<sup>1</sup>. It reflects how well a material can get rid of the energy. Ideal elastic material show no  $\tan \delta$ , whereas viscous materials exhibit high values of  $\tan \delta$ .  $\tan \delta$  values higher than 1 represent liquid-like regions, contrarily to  $\tan \delta$  values smaller than 1, that represent gel-like behavior to solid-like behavior, as  $\tan \delta$

approaches zero<sup>51</sup>. These  $\tan \delta$  values were clearly observed at the 3-D contour map (Fig. 1F) and became identified with the greenish-blue traces mostly concentrated at the centre of the image (Fig. 1D). Polly *et al.* (2012) obtained 0.0092 GPa of  $\tan \delta$ , different from the present results. Because bone is a composite material comprising mineral, organic material (Fig. 2) and water, its viscoelastic properties may be influenced by all or some of these components or by their interactions<sup>1</sup>. Generally, values reported for bone properties in the literature vary, mainly due to differences between the studies in anatomical location, hydration/embedding techniques, and testing parameters. The intratrabecular variation in intrinsic material properties may also affect nanoindentation measurements. Variations may be due to testing nanoscale structures in a hierarchical organised material that extends to the micro level<sup>2</sup>.

The elastic behavior characterised as the elastic energy stored which is released after deformation, *i.e.*, the storage modulus ( $E'$ ) was 13.75 GPa (Table 1), represented at Fig. 1C as green traces throughout the whole image. The yellow and reddish figures discovered at the top half of the image corresponded to high viscoelastic properties and could be a result of the increase in concentration of collagen fibrils (Fig. 2), whose diameter was approximately 830 nm (Table 1). This great viscoelasticity was an outcome of high stored potential energy available for elastic recoil<sup>52</sup>. Polly *et al.* (2012) obtained 15.56 GPa of  $E'$ , close to our results. This was an expected result because it is the mineral phase that is principally responsible for the storage modulus<sup>1</sup>. Trabecular bone microarchitecture is compromised in postmenopausal women and is associated with declining trends in storage modulus. Macroscopic DMA testing has also shown that dehydration increases the storage modulus<sup>53</sup> and decreases the loss tangent<sup>54</sup>. In the present study, hydration state was maintained through the complete procedure, so the

relative degree of wetness may have conditioned our results. Loss tangent and loss modulus generally increased but with varying levels of significance <sup>2</sup>.

Any resulting phase lag between the force applied and the displacement is related to a loss of energy known as the loss modulus or damping  $E''$ .  $E''$  is a measure of the energy dissipation of a material under cyclic load<sup>15</sup>. Dissipation of energy within the structures is of prime importance in dynamic systems <sup>47</sup> such as the bone. The loss modulus values (in general low), support the fact that those structures are not elastic brittle solids <sup>52</sup>. In the present research, the trabecular bone attained 6.39 GPa of loss modulus, referred at the scanning analysis (Fig. 1B) as the green-bluish traces. Polly *et al.* (2012) obtained 0.164 GPa of  $E''$ . Uncertainties in the measurement of bone tissue by nanoindentation, including the influences of sample preparation, tissue heterogeneity, and anisotropy, may have accounted to explain differences.

## **Conclusions**

The goal of the present study was to propose a study protocol on trabecular bone, based on nanoindentation and AFM characterisation, in order to assess degenerative bone diseases and bone quality with the aim of evaluating new therapies. This study poses a first approach to the measurement of bone quality in postmenopausal trabecular bone by combining quasi-static, nano-DMA analysis and tribology of dentin surface through AFM characterization. In future works, it should be determined the balance between microdamage accumulation, cracks and repair in bone mass and their influence on mechanical properties with specific medication over longer time periods. Future studies which connect nanoindentation measurements with local mineralisation state will help to clarify some outcomes. Moreover, further work is required to determine the

microstructural sources of these differences, such as lamellar/collagen organisation and orientation, mineralisation, and failure modes.

### **Conflict of interest**

The authors state that none of them has a conflict of interest that relates to the content discussed in this manuscript.

All authors disclose any financial and personal relationships with other people or organisations that could inappropriately influence their work.

### **Acknowledgements**

Project MAT2017-85999-P supported by the Ministry of Economy and Competitiveness (MINECO) and European Regional Development Fund (FEDER).

### **References**

1. Yamashita J, Furman BR, Rawls HR, Wang X, Agrawal CM. The use of dynamic mechanical analysis to assess the viscoelastic properties of human cortical bone. *J Biomed Mater Res* 2001;58: 47-53.
2. Polly BJ, Yuya PA, Akhter MP, Recker RR, Turner JA. Intrinsic material properties of trabecular bone by nanoindentation testing of biopsies taken from healthy women before and after menopause. *Calcif Tissue Int* 2012;90: 286-93.
3. Jiroušek O. Nanoindentation of Human Trabecular Bone-Tissue Mechanical Properties compared to Standard Engineering Test Methods, *Nanoindentation in Materials Science*. Dr. Jiri Nemecek (Ed.), In Tech; 2012.

4. Bayraktar HH, Gupta A, Kwon RY, Papadopoulos P, Keaveny TM. The modified super-ellipsoid yield criterion for human trabecular bone. *J Biomech Eng* 2004;126: 677-84.
5. Poon B, Rittel D, Ravichandran G. An analysis of nanoindentation in linearly elastic solids. *Int J Solids Struct* 2008;45: 6018-33.
6. Balooch M, Habelitz S, Kinney JH, Marshall SJ, Marshall GW. Mechanical properties of mineralized collagen fibrils as influenced by demineralization. *J Struct Biol* 2008;162: 404-410.
7. Bar-On B, Wagner HD. Elastic modulus of hard tissues. *J Biomech* 2012;45: 672-8.
8. Hu S, Li J, Liu L, Dai R, Sheng Z, Wu X, et al. Micro/Nanostructures and Mechanical Properties of Trabecular Bone in Ovariectomized Rats. *Int J Endocrinol* 2015;2015: 252503.
9. Swadener JG, Rho JY, Pharr GM. Effects of anisotropy on elastic moduli measured by nanoindentation in human tibial cortical bone. *J Biomed Mater Res* 2001;57: 108–112.
10. Rho J, Currey JD, Zioupos P, Pharr GM. The anisotropic Young's modulus of equine secondary osteones and interstitial bone determined by nanoindentation *J Exp Biol* 2001;204: 1775–1781.
11. Hengsberger S, Enstroem J, Peyrin F, Zysset Ph. How is indentation modulus of bone related to its macroscopic elastic response? A validation study. *J Biomech* 2003;36: 1503–1509.

12. Yuya PA, Amborn EK, Beatty MW, Turner JA. Evaluating anisotropic properties in the porcine temporomandibular joint disc using nanoindentation. *Ann Biomed Eng* 2010;38: 2428–2437.
13. Ojanen X, Isaksson H, Töyräs J, Turunen MJ, Malo MKH, Halvari A, et al. Relationships between tissue composition and viscoelastic properties in human trabecular bone. *J Biomech* 2015;48: 269-275.
14. Wang X, Bank RA, TeKoppele JM, Agrawal CM. The role of collagen in determining bone mechanical properties. *J Orthop Res* 2001;19: 1021-6.
15. Hayot CM, Forouzesh E, Goel A, Avramova Z, Turner JA. Viscoelastic properties of cell walls of single living plant cells determined by dynamic nanoindentation. *J Exp Bot* 2012;63: 2525-40.
16. Rettler E, Hoepfener S, Sigusch BW, Schubert US. Mapping the mechanical properties of biomaterials on different length scales: depth-sensing indentation and AFM based nanoindentation. *J Mater Chem B* 2013;1: 2789-806.
17. Habelitz S, Balooch M, Marshall SJ, Balooch G, Marshall GW. In situ atomic force microscopy of partially demineralized human dentin collagen fibrils. *J Struct Biol* 2002;138: 227-36.
18. Pathak S, Vachhani SJ, Jepsen KJ, Goldman HM, Kalidindi SR. Assessment of lamellar level properties in mouse bone utilizing a novel spherical nanoindentation data analysis method. *J Mech Behav Biomed Mater* 2012;13: 102-17.
19. Erben RG. Embedding of Bone Samples in Methylmethacrylate: An Improved Method Suitable for Bone Histomorphometry, Histochemistry, and Immunohistochemistry. *J. Histochem Cytochem* 1997; 45:307–313.

20. Xu J, Rho JY, Mishra SR, Fan Z. Atomic force microscopy and nanoindentation characterization of human lamellar bone prepared by microtome sectioning and mechanical polishing technique. *J Biomed Mater Res A* 2003;67: 719–726.
21. Lane NE, Yao W, Balooch M, Nalla RK, Balooch G, Habelitz S, et al. Glucocorticoid-treated mice have localized changes in trabecular bone material properties and osteocyte lacunar size that are not observed in placebo-treated or estrogen-deficient mice. *J Bone Miner Res* 2006;21: 466-76.
22. Balooch G, Yao W, Ager JW, Balooch M, Nalla RK, Porter AE, et al. The aminobisphosphonate risedronate preserves localized mineral and material properties of bone in the presence of glucocorticoids. *Arthritis Rheum* 2007;56: 3726-37.
23. Han L, Grodzinsky AJ, Ortiz C. Nanomechanics of the Cartilage Extracellular Matrix. *Annu Rev Mater Res* 2011;41: 133-68.
24. Toledano M, Aguilera FS, Cabello I, Osorio R. Remineralization of mechanical loaded resin-dentin interface: a transitional and synchronized multistep process. *Biomech Model Mechanobiol* 2014;13: 1289-302.
25. Hertz H. Über die Berührung fester elastischer Körper (On the contact of rigid elastic solids). *J Reine Angew Math* 1881;92: 156-171.
26. Macosko CW. *Rheology: Principles, Measurements, and Applications*. New York: VCH; 1994.
27. Oliver WC, Pharr GM. An improved technique for determining hardness and elastic modulus using load and displacement sensing indentation experiments. *J Mater Res* 1999; 27:1564–1583.

28. Takeyasu K, Omote H, Nettikadan S, Tokumasu F, Iwamoto-Kihara A, Futai M. Molecular imaging of Escherichia coli F<sub>0</sub>F<sub>1</sub>-ATPase in reconstituted membranes using atomic force microscopy. *FEBS Lett* 1996;392: 110-3.
29. Hengsberger S, Kulik A, Zysset Ph. A combined atomic force microscopy and nanoindentation technique to investigate the elastic properties of bone structural units. *Eur Cells Mater* 2001;1: 12–17.
30. Hengsberger S, Ammann P, Legros B, Rizzoli R, Zysset P. Intrinsic bone tissue properties in adult rat vertebrae: modulation by dietary protein. *Bone* 2005;36:134–141.
31. Wang X, Rao DS, Ajdelszta L, Ciarelli TE, Lavernia EJ, Fyhrie DP. Human iliac crest cancellous bone elastic modulus and hardness differ with bone formation rate per bone surface but not by existence of prevalent vertebral fracture. *J Biomed Mater Res B* 2008; 85:68–77.
32. Franzoso G, Zysset PK. Elastic anisotropy of human cortical bone secondary osteons measured by nanoindentation. *J Biomed Eng* 2009;131: 021001–021011.
33. Rho JY, Tsui TY, Pharr GM. Elastic properties of human cortical and trabecular lamellar bone measured by nanoindentation. *Biomaterials* 1997;18: 1325–1330.
34. Rho JY, Roy MEI, Tsui TY, Pharr GM. Elastic properties of microstructural components of human bone tissue as measured by nanoindentation. *J Biomed Mater Res A* 1999;45: 48–54.
35. Zysset PK, Guo XE, Ho-er CE, Moore KE, Goldstein SA. Elastic modulus and hardness of cortical and trabecular bone lamellae measured by nanoindentation in the human femur. *J Biomech* 1999;32: 1005–1012.

36. Hensberger S, Kulik A, Zysset Ph. Nanoindentation discriminates the elastic properties of individual human bone lamellae under dry and physiological conditions. *Bone* 2002;30: 178–184.
37. Oyen ML, Ferguson VL, Bembey AK, Bushby AJ, Boyde A. Composite bounds on the elastic modulus of bone. *J Biomech* 2008;41: 2585–2588.
38. Fratzl-Zelman N, Roschger P, Gourrier A, Weber M, Misof BM, Loveridge N, et al. Combination of nanoindentation and quantitative backscattered electron imaging revealed altered bone material properties associated with femoral neck fragility. *Calcif Tissue Int* 2009; 85: 335–343.
39. Ferguson VL, Bushby AJ, Boyde A. Nanomechanical properties and mineral concentration in articular calcified cartilage and subchondral bone. *J Anat* 2003;203: 191–202.
40. Bembey AK, Oyen ML, Bushby AJ, Boyde A. Viscoelastic properties of bone as a function of hydration state determined by nanoindentation. *Philos Mag* 2006;86: 5691-5703.
41. Donnelly E, Baker SP, Boskey AL, van der Meulen MCH. Effects of surface roughness and maximum load on the mechanical properties of cancellous bone measured by nanoindentation. *J Biomed Res A* 2006;77: 426–435.
42. Paietta RC, Campbell SE, Ferguson VL. Influences of spherical tip radius, contact depth, and contact area on nanoindentation properties of bone. *J Biomech* 2011;44: 285–290.
43. Morris MD, Mandair GS. Raman assessment of bone quality. *Clin Orthop* 2011;469: 2160-9.

44. Yerramshetty JS, Lind C, Akkus O. The compositional and physicochemical homogeneity of male femoral cortex increases after the sixth decade. *Bone* 2006;39: 1236-43.
45. Ryou H, Romberg E, Pashley DH, Tay FR, Arola D. Importance of age on the dynamic mechanical behavior of intertubular and peritubular dentin. *J Mech Behav Biomed Mater* 2015;42: 229-42.
46. Ryou H, Pashley DH, Tay FR, Arola D. A characterization of the mechanical behavior of resin-infiltrated dentin using nanoscopic Dynamic Mechanical Analysis. *Dent Mater* 2013;29: 719-28.
47. Agrawal R, Nieto A, Chen H, Mora M, Agarwal A. Nanoscale damping characteristics of boron nitride nanotubes and carbon nanotubes reinforced polymer composites. *ACS Appl Mater Interfaces* 2013;5: 12052-7.
48. Misra A, Spencer P, Marangos O, Wang Y, Katz JL. Micromechanical analysis of dentin/adhesive interface by the finite element method. *J Biomed Mater Res B Appl Biomater* 2004;70: 56-65.
49. Mashiba T, Turner CH, Hirano T, Forwood MR, Johnston CC, Burr DB. Effects of suppressed bone turnover by bisphosphonates on microdamage accumulation and biomechanical properties in clinically relevant skeletal sites in beagles. *Bone* 2001;28: 524-31.
50. Espino DM, Shepherd DE, Hukins DW. Viscoelastic properties of bovine knee joint articular cartilage: dependency on thickness and loading frequency. *BMC Musculoskelet Disord* 2014;15: 205

51. Winter HH. Can the gel point of a cross-linking polymer be detected by the  $G' - G''$  crossover? *Polym Eng Sci* 1987;27: 1698-1702.
52. Balooch G, Marshall GW, Marshall SJ, Warren OL, Asif SA, Balooch M. Evaluation of a new modulus mapping technique to investigate microstructural features of human teeth. *J Biomech* 2004;37: 1223-32.
53. Bushby A, Ferguson V, Boyde A. Nanoindentation of bone: comparison of specimens tested in liquid and embedded in polymethylmethacrylate. *J Mater Res* 2004;19:249–259
54. Yamashita J, Li X, Furman BR, Rawls HR, Wang X, Agrawal CM. Collagen and bone viscoelasticity: a dynamic mechanical analysis. *J Biomed Mater Res A* 2002;63: 31–36.

**Table 1.** Nano-DMA analysis: Mean and standard deviation of complex modulus (GPa),  $\tan(\delta)$ , loss and storage modulus (GPa). AFM analysis: Mean and standard deviation of nanoroughness (SRa) (nm), fibrils width (nm), nanohardness (GPa) and young modulus (GPa). Presented variables were measured on trabecular bone.

Nano-DMA analysis				AFM analysis			
CM ( $E^*$ )	Tan ( $\delta$ )	LM ( $E''$ )	SM ( $E'$ )	SRa	Fibrils width	Nanohardness	Young modulus
17.94 (3.15)	0.62 (0.10)	6.39 (1.28)	13.75 (3.21)	101.07 (23.71)	831.28 (73.90)	0.145 (0.036)	2.95 (0.73)

Abbreviations: CM: Complex Modulus, LM: Loss Modulus, SM: Storage Modulus; AFM: Atomic Force Microscopy; DMA: Dynamic Mechanical Analysis

## Legend of figures

**Figure 1**, Nano-DMA analysis in trabecular bone. **Fig. 1A**, scanning mode nano-DMA analysis of the map of the complex modulus ( $E^*$ ) in trabecular bone. In the color scheme shown, the redder color corresponds to the highest values of complex modulus  $E^*$ . The average resistance to deformation was attained around the yellow-greenish zones ( $\sim 18$  GPa). **Fig. 1B**, scanning mode nano-DMA analysis of the map of the loss modulus ( $E''$ ) in trabecular bone. In the color scheme shown, the redder color corresponds to the highest values of loss modulus  $E''$ . The average ability to dissipate energy at the trabecular bone was achieved close to the green areas ( $\sim 6.4$  GPa). **Fig. 1C**, scanning mode nano-DMA analysis of the map of the storage modulus ( $E'$ ) in trabecular bone. In the color scheme shown, the red color corresponds to high values of the locally measured moduli. The average energy stored in the trabecular bone occurred at greenish regions ( $\sim 13.7$  GPa). **Fig. 1D**, scanning mode nano-DMA analysis of the map of the  $\tan \delta$  in trabecular bone. In the color scheme shown, the redder color corresponds to higher values of the locally measured moduli. The average proportion of energy available at the trabecular bone coincides with the bluish green areas ( $\sim 0.6$  GPa). **Fig. 1E**, 3-D contour map of the complex modulus ( $E^*$ ) distribution in trabecular bone ( $\sim 12$  GPa). The dark color corresponds to low values and the red color to the highest values of the locally measured complex modulus ( $E^*$ ). **Fig. 1F**, 3-D contour map of the  $\tan \delta$  distribution in trabecular bone ( $\sim 1$  GPa). The dark color corresponds to low values and the red color to the highest values of the locally measured  $\tan \delta$ . In this figure, the values of  $\tan \delta$  were used to map out a subsurface pore (pointer) in the wet trabecular bone that is characterised by a large viscous response, surrounding it (arrows). Magnitudes of X, Y and Z axis of Figures E and F are in microns.

**Figure 2**, AFM images of trabecular bone. 30 x 30  $\mu\text{m}$  top-view (**Figs. 2A, 2C**) and surface plot image (**Figs. 2B, 2D**) of trabecular bone, showing the region of interest: prominent mineral deposits (arrows), limiting mineral-depleted areas (pointers). The collagen fibers and mineral crystals were packed in trabeculae and presented as nodular-like surfaces. Bundles combining fibrillar collagen and embedded minerals (faced arrows) may be observed. Light areas correspond to high zones on the sample surface.

Figure 1

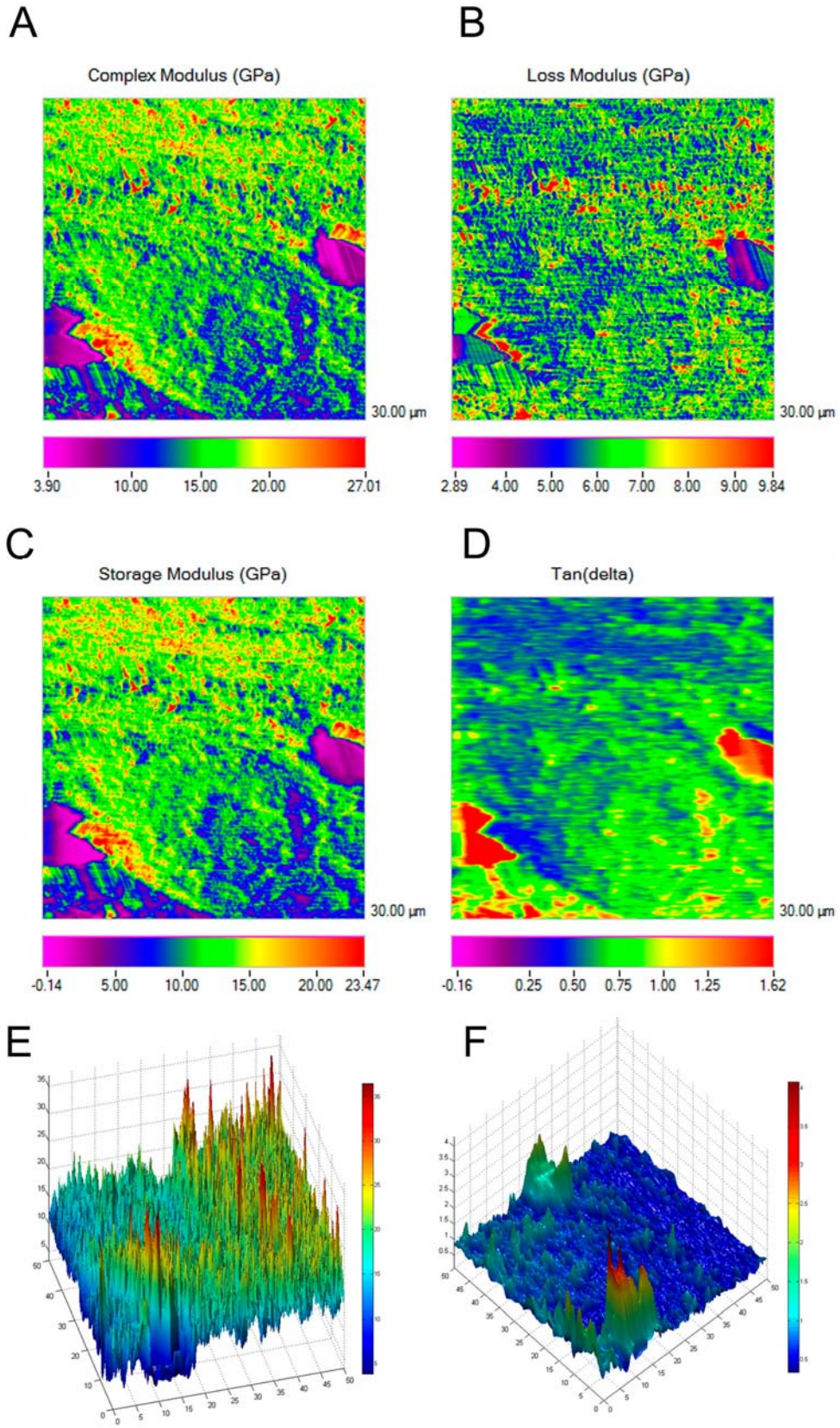
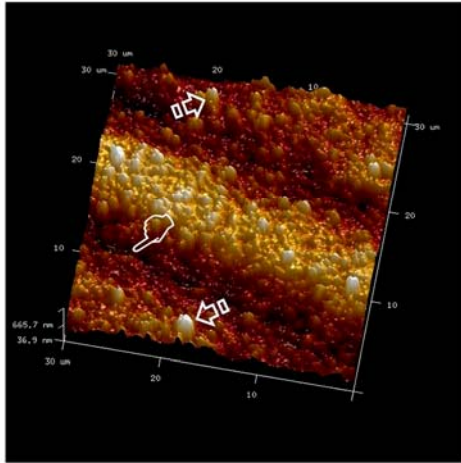
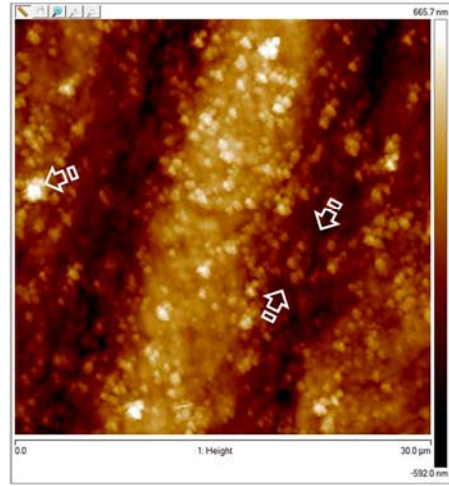


Figure 2

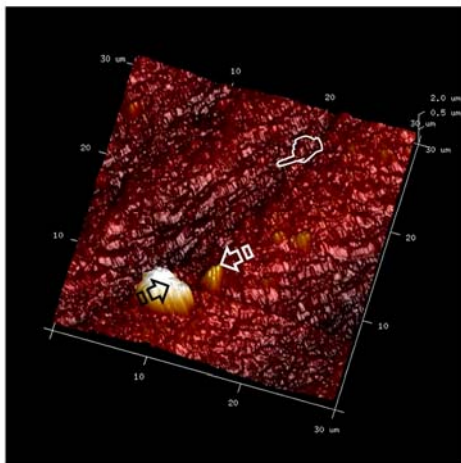
A



B



C



D

